Automated Instrumentation for Continuous Monitoring of the Dielectric Properties of Woody Vegetation: System design, implementation and selected *in situ* measurements

Kyle C. McDonald *, Reiner Zimmerman †, JoBea Way * and William Chun*

* Mail Stop 300-233
Jet Propulsion I Laboratory
California Institute of '1'ethnology
4800 Oak Grove Drive
Pasadena, CA 91109-8001, U.S.A.
Phone: (818) 351-3263
FAX: (S1S) 354-9476
email: kyle.mcdonald@jpl.nasa.gov

† Bayreuth Institute for Terrestrial Ecosystem Research
(111"1'01<)
The University of Bayreuth
Dr. H. Frisch Str. 1
D-95448 Bayreuth, Germany

Abstract – Design and implementation of a system for the automated and continuous *in situ* monitoring of the dielectric constant, of woody vegetation tissue is presented. Implementation of both single channel and multi-channel systems is discussed. These systems permit unsupervised continuous and long-term monitoring of vegetation canopy dielectric behavior in remote field sites. Utilizing open- ended coaxial lines, the real and imaginary parts of microwave dielectric constant of woody plant tissue are inferred from direct measurement of the magnitude and phase of the microwave reflection coefficient. A sample of *in situ* data obtained from three field studies is presented. These examples demonstrate that measurements obtained with our systems allow new insight into the dielectric behavior of vegetation with respect to the physiological and hydraulic function of trees. The observations provide a significant advance in our ability to link canopy physiological and hydraulic behavior to radar remote sensing observations.

1 Introduction

Past research has demonstrated that significant variations in dielectric properties of trees (ϵ_{tree}) occur during changes in tree canopy water status (Ψ_{tree}) [20, 21, 31, 42, 46]. Radar backscatter from tree canopies is influenced by canopy structure and dielectric properties. A tree's dielectric properties are in turn influenced by canopy water status. Therefore it is possible that useful information concerning long and short term variations in Ψ_{tree} may be observed remotely with synthetic aperture radar (SAIL). If a link between ϵ_{tree} and Ψ_{tree} can be made, radar then offers a unique capability to monitor changes in Ψ_{tree} from spaceborne platforms. This would permit large scale regional mapping of diurnal, weekly and seasonal variations within ecosystems that are caused by changes in hydraulic parameters related to vegetation and soil freeze/thaw state, canopy water content, and xylem water potential.

'Two distinct problems must be addressed to develop techniques for remotely monitoring canopy water status and associated physiological properties. First, the relationship between canopy dielectric properties and radar backscatter must be well understood. This has been addressed over the past years through field experiments and development of theoretical backscattering models [5, 11, 16, 1 i', 2S, 33, 35, 38, 43]. Second, the relationship between the dielectric constant of the canopy constituents and their associated physiological parameters must be understood. Models that relate vegetation water content to dielectric constant under static laboratory conditions have been developed [36]. However, in *situ* observations

of vegetation dielectric behavior indicate a highly dynamic time-varying behavior which is more complex than accounted for by existing static vegetation dielectric models. It is well understood that dielectric constant depends directly on vegetation water content. However *in vivo* measurements of dielectric constant have shown more significant variability than can be accounted for through changes in water content of living plant tissue alone ['20, 46]. Significant changes in dielectric properties will affect radar backscatter. The key to exploiting radar as an instrument- for monitoring vegetation canopy hydraulic properties lies in developing an understanding of the relationship between canopy hydraulic changes and dielectric constant.

The average dielectric constant (ϵ_r) of a vegetation constituent relates to a composite of various structurally and physiologically different plant components. For each constituent, ϵ_r is sensitive to such plant physiological parameters as tissue water content, the proportion of bound to free water, its electrolytic composition, and hydraulic plant water potential. The vegetation water status and thus ϵ_r changes diurnally and seasonally. Monitoring of ϵ_r in various plant tissue's permits the unraveling of interactions between ϵ_{tree} and Ψ_{tree}. A functional model $\epsilon = f(\Psi)$ may thus be developed which allows ecologists and climate modelers to obtain large scale information about vegetation water status for studies of energy balance. water exchange, nutrient uptake and carbon balance within the soil- plant -atmosphere continuum [44].

The largest water-containing component of mature trees is the trunk. As tree

trunks have a complex, multi-layered anatomy, the dielectric constant varies with depth from the bark surface [25]. Figure 1 is an illustration of the different anatomical layers of a typical dicotylous tree bole. The outer layers include the bark and tile bast which are protective layers with very low dielectric constant. The bast cambium, the phloem, and the cambium are high dielectric regions consisting of a thin layer of cells through which proteins and carbohydrates are actively transported in aqueous solution from the canopy to the roots. Beneath the phloem is the hydroactive xylem through which water and minerals move in small vessels from the roots to the canopy [24, 30]. The inner tree core with its inactive xylem acts primarily as a tree support structure and as a long term water storage compartment [40]. Conifers have a similar anatomical arrangement of functional layers, but xylem vessel diameters are generally smaller and hydraulic flux resistances are larger. Monocotylous trees such as palms and yucca have evenly distributed units of phloem/xylem throughout the stem cross sect ion.

To investigate the response of dielectric properties to canopy physiological parameters, and to understand the links between plant physiology and temporal changes in radar backscatter, it is necessary to document the status and change in vegetation dielectric and physiological properties. Our efforts have thus been directed toward the understanding of three key issues:

1. Dielectric constant of plants as influenced by changes in plant water status

   Work on understanding the dielectric properties of plant tissue has been clone using both modeling approaches as wells as measurements on isolated plants

[s, 9,12, *11,* 15, 20,27, 31, 34]. Vegetation dielectric constant is influenced mainly by the tissue water content. The role of chemicals in solution (salinity) is well investigated [37] and confirms that dielectric constant must vary with changes in osmolarity as well. However, the plant leaf tissues and other structural components (trunks and branches) represent spatially highly variable arrays of proteins, carbohydrates, and bound and free water in xylem vessels and living cells.

2. Short term and diurnal changes in vegetation dielectric constant

Plant water potential characterizes the actual water availability for plants and influences their carbon uptake capability. Models have been under development such that, when linked with the measurement of environmental parameters, the water loss of entire forest stands as well as their carbon uptake can be estimated [3, 6]. The knowledge of stand transpiration and the ability to derive canopy conductance of water vapor on a regional scale provides essential information for global climate simulations and models (GCMs). Direct measurement of water potential of large plant communities by remote sensing techniques would close a gap in our ability to drive such models with directly measured parameters.

3. Long term (seasonal) variations of vegetation dielectric constant

Accurate information on the length of growing season significantly improves estimates of annual carbon exchange in high latitude regions. For evergreen

conifers of the boreal region, the frost-free period bounds the growing season length and the duration of the period of significant CO_2 uptake by photosynthesis. Furthermore, both coniferous and deciduous tree types are driven in their long term growth potential by the length of time during which active mineral and water uptake through the soil-root continuum is possible. Estimating the annual time span during which favorable soil temperature regimes persist is likely to be of moue ecological significance than determination of the temperature regime of the above-groulld biomass. Measurements collected in Alaska and Canada by the NASA/JPL AIRSAR and the ERS-1 SAR show' that regional freezing results in a significant drop in radar backscatter. This drop is caused by a sharp decrease in soil and canopy dielectric constant as the water in the vegetation and organic soil freezes [29, 44, 45]. To address the use of imaging radar for estimating growing season length, the relationship between canopy, bole, and soil freezing, and the beginning and end of seasonal photosynthetic activity must be ascertained together with the sensitivity of spaceborne imaging radar backscatter to freeze/tlla\v processes within the vegetation and organic soil.

Documentation of the status ancl change in vegetation dielectric properties and water status necessitates the development of a stable and reliable capability for *in situ* measurement of ϵ_r. The field portable dielectric probe (PDP) developed by Applied Microwave Corporation [2, 4] has been used to characterize microwave dielectric properties of vegetation and soil in many remote sensing studies. Figure

2 is a system-level block diagram of the hand-held PDP unit. The probe consists of a reflectometer and a signal processing assembly. The open-ended coaxial probe tip that terminates the measurement cable is placed in contact with the dielectric medium, or test sample. The reflection coefficient (amplitude and phase) as measured at the probe tip is determined from the output of a comparator circuit that compares the signal reflected from the test sample to that reflected from the open-ended coaxial reference cable. For proper operation, the cables of each reflectometer channel are phase trimmed so that the reference and measurement channels are of nearly identical electrical length. The comparator output voltages are digitized in the signal processing assembly by an 8 bit A/I) converter and stored on an 11P-41 band held computer. The test material's dielectric constant is inferred from the measured reflection coefficient through application of an equivalent circuit model relating these quantities to parameters derived from reflection coefficient measurements taken on a set of reference materials of known dielectric constants.

To measure the dielectric constant of one of the anatomical layers of a tree bole with a PDP, a hole is drilled into the trunk at the location and to the depth desired. Before inserting the measurement tip, a reference calibration is obtained to account for system drifts induced by temperature changes or flexing of the RF measurement cable. Air is generally used as the reference medium. The open-ended coaxial probe tip is then placed in contact with the measured tissue and slight pressure is applied by the operator to ensure good contact between the probe

tip and the tissue. A series of several consecutive measurements is performed and averaged to obtain a single estimate of dielectric constant at a single depth and single point in time. Measurements may be stored in the hand held computer for post processing and analysis.

A typical dielectric profile of a tree trunk (dielectric constant as a function of depth) is shown in Figure 3. These measurements were made of a white spruce tree with trunk diameter at breast height of about 35 cm at the Bonanza Creek Experimental Forest, Alaska during March 1988 while the trees were in a thawed state [41, 44]. The peaks observed in both the real and imaginary parts of the dielectric constant at depths between 1-4 cm correspond to the phloem and potentially hydroactive xylem tissues. The bark and permanently hydropassive xylem have relatively low dielectric constants because they contain little free water as compared to the phloem and hydroactive xylem regions.

The PDP was designed to provide a field-portable capability for *in situ* measurement of dielectric constant. However, tile hand-held unit is inefficient for obtaining the large amounts of data required to accurately characterize the temporal and spatial dynamics of ϵ_{tree} and relating these observations to vegetation physiology. Obtaining the large amount of repeated measurements necessary to accurately characterize this relationship is extremely time and labor intensive and requires personnel to be in continuously in the field.

The accuracy of the data acquired with the PDP is dependent on the operator's ability to repeat measurements with consistent technique. The hand held

computer that serves as the user interface severely limits the ability of the instrument to store large amounts of *in situ* measurements. Another limitation of the portable probe is that for accurate measurement, tile reference calibration procedure must be periodically repeated, requiring removal of the measurement tip from the observed medium. This limits the ability to discriminate more subtle changes in dielectric constant *in situ* without perturbing the measurement tip/tissue geometry. Changes in tip/tissue geometry and in the pressure applied to the PDP probe tip by the operator during measurement can introduce significant variations in the resulting estimates of ϵ_r. To avoid such problems, large spatial samples may be acquired. However this approach is limited in plants because of naturally occurring spatial variations and because damage to the plant tissue caused by the repeated measurement processes eventually alters the tissue's performance.

In this paper, we present the design and implementation of a dielectric measurement system (DMS) that allows the automated, simultaneous, and continuous *in situ* monitoring of the dielectric properties of vegetation canopy constituents. Our design effort was undertaken to overcome the limitations of measurement geometry variations and repeated manual calibration, to facilitate the measurement scheme necessary to carry out experiments involving continuous or long-term monitoring of tree dielectric properties, and to allow the use of multiple probes for proper statistical design of experiments. Utilizing the open-end coaxial line measurement technique implemented with the 1'1)1', this system facilitates long-term continuous monitoring of canopy dielectric properties. Systems have been constructed to

monitor reflection coefficient, at P-band (0.45 GHz), L-band (1.2 GHz) and C-band (5 GHz). These frequencies were chosen to coincide with frequencies of existing airborne and spaceborne radar systems and to allow use of electronics implemented in available PDP units. Sections 2 and 3 of this paper review details of designs, installation and operation of the measurement systems. The DMS has been deployed at several field sites together with instrumentation for monitoring canopy physiological parameters during a number of experiments. We provide some examples of concurrent measurements of ϵ_{tree} and Ψ_{tree} in Section 4.

2 System Design

The dielectric monitoring system (DMS) developed for this application incorporates a PDP unit with switching network and data logger assemblies that permit autonomous monitoring of dielectric constant in a near-continuous fashion [18, 19]. Both single- and multi-channel systems have been developed and tested in field experiments. Figure 4 is a system-level block diagram of the single-challnel DMS. This unit consists of one PDP augmented with a Delta-T Devices data logger and a custom-built measurement/calibration switch assembly. The measurement cable of the PDP is connected directly to the switch assembly which consists of a microwave switch and two open-ended coaxial probe tips. The measurement tip is implanted into the test medium (*e.g.* a tree trunk) and the reference calibration tip is suspended in an air tight vial containing a small amount of desiccant to keep the air in the vial dry. This tip is used for reference air calibration readings and

for system calibration checks performed against calibration standards with the dry air vial removed. The electrical length of the reference cable within the RF measurement head must be modified to account for the change in the electrical length of tile measurement cable/tip combination caused by the addition of the switch assembly.

For each measurement sample, the data logger stores three channels of information: (1) the reflection coefficient magnitude, (2) the reflection coefficient phase, and (3) the tip assembly switch position. Switching of the DMS assembly between measurement and calibration tips is controlled through an interface with a switch control unit that is commanded by a control signal supplied by a data logger relay. With the data logger relay open, the tip assembly is in the calibration position; when the relay is c1oscc1, the assembly switches to tile measurement position. Position of the switch is monitored by the logger through a switch position indicator signal supplied by the switch control unit. The reflection coefficient measurement is supplied to the logger through an analog signal interface with the PDP that provides the pre-processed analog voltages corresponding the magnitude and phase of the reflection coefficient. These data are digitized in the data logger by a 12 bit A/D converter, providing improved resolution over the 8 bit A/D converter in the PDP processor assembly.

The timing of the switch assembly toggling and the sampling rate of the data are programmed by the user into the logger system software and stored in the logger memory. The logger used in our system (Delta-T Devices data logger with full

memory extension) is capable of storing more than 120,000 individual readings, corresponding to over 40,000 sets of reflection coefficient/switch position observations. Thus, if an adequate power source is available in the field (*e.g.* a bank of 12 volt batteries charged by a set of solar panels). it is possible to deploy One of these systems in a remote area for several months and obtain autonomous long-term measurements of the temporal dynamics of dielectric constant for a single canopy constituent.

Figure 5 is a system-level block diagram of the multi-channel dielectric monitoring system. This unit operates on the same principle as the single channel unit, but it also incorporates a multiplexing scheme for monitoring several channels of dielectric measurements with a single PDP unit. Tllulti-channel units constructed so far have incorporated an eight channel multiplexing scheme, thus each is referred to as an "octopus." The multiplexing unit consists of a switch control unit that operates a microwave switching network. The switching' net work Switches the measurement and reference channels of the PDP comparator circuitry in tandem between pairs of measurement and reference cables. Each measurement cable is connected to a single measurement/calibration switch assembly. Each reference cable must be trimmed to the same electrical length as the corresponding measurement channel to allow for proper operation of the PDP comparator circuit. The switching network steps in sequence among the measurement/reference cable pairs. allowing the PDP unit to monitor a number of independent measurement/calibration switch assemblies and thus permitting autonomous monitoring of several canopy

constituents in a near-simultaneous fashion.

The switch control unit internal to the multiplexing unit operates both the microwave switching network and each of the measurement/calibration switch assemblies. The control unit also interfaces with the data logger through a set of control and communication cables. These cables carry signals from the logger relays, commanding the operation of the microwave switching network and the measurement/calibration switch assemblies. The data logger records the preprocessed analog signal from the PDP unit (magnitude and phase of the reflection coefficient) along with a signal from the switch control unit that indicates the positions of the switching network and the corresponding measurement/calibration switch assembly.

3 System Installation and Calibration

System tests and *in situ* measurements utilizing the octopus as well as single channel DMS units were performed as part of field experiments in various climatic regions. Figures 6 - 8 are photographs of various components of an octopus and its installation site at the Bonanza Creek Experimental Forest (BCEF), near Fairbanks, Alaska. Figure 6 shows an eight channel multiplexing unit and a measurement/calibration switch assembly. The measurement and reference channels of the interfacing PDP's RF comparator circuitry connect to the two SMA style connectors on the far right hand side of the multiplexing unit. The system is powered by a bank of 12 volt DC batteries charged with a set of solar panels.

To monitor the dielectric behavior of a tree trunk, a hole is drilled to the desired depth, a measurement probe is inserted with an attached measurement/calibration switch, and the assembly is strapped to the tree (Fig. 7a). The coaxial probe tips employed for these measurements have a center electrode extended about 1 mm beyond the outer probe shielding. This type of probe geometry has been shown to improve probe contact with the measured medium while increasing the probe's effective measurement volume and still allowing accurate characterization of an acceptable range of dielectric constant values [23, 32]. Inserting tile probe to a depth of 0.,5-1 cm into the wood assures good mechanical support for the assembly while still allowing placement within tile trunk's hydroactive tissue. Before installation, profiles of dielectric constant vs. depth (Fig. 3) may be measured and tree core samples may be taken to verify the extent of the hydroactive xylem tissue and to determine the optimal insertion depth of the measurement probe. 'l'he measurement ant! switch control cables and the reference calibration tip are then connected to the switch assembly (Fig. 7b). In order for the system to obtain accurate reference calibrations for each measurement series, it is important that the calibration tip be the same type and size as the measurement tip so that the two tips have identical electrical characteristics.

As installed at the BCEF test site, the octopus monitored the dielectric behavior of several trees (Fig. 8). A single measurement/calibration switch assembly was installed on each monitored tree. The measurement/reference cable pairs were run to each switch assembly together with a switch control cable inside PVC pipes

to protect the cables from direct exposure to weather and damage from wildlife. After the octopus is in place, each reference cable is trimmed to the same electrical length as its corresponding measurement cable/measurement switch assembly to allow proper operation of the PDPRF comparator circuitry. The switch assemblies are then covered with a protective sheet of plastic insulation.

Each system channel must be calibrated so that dielectric constant may be computed from the reflection coefficient measurements. This is accomplished by taking readings of reflection coefficient on a series of calibration standards of known dielectric constant. We use a selection of alcohols and solvents as calibration standards. The reference tip allows periodic calibration checks during equipment servicing.

The calibration procedure is identical to that used to calibrate the hand-held PDP units and is discussed in detail by Dobson [7] and in the PDP users' manual [2]. The procedure is based on application of an equivalent circuit model that relates the dielectric constant of the substance placed in contact with tile probe tip to that of a capacitor filled with a material of equivalent dielectric constant. Applying this equivalent circuit model to the probe measurement yields a straightforward relationship that relates two transformation variables (TranR and TranI) to the voltage output of the PDP unit:

$$\text{TranR} = \frac{-2\,|V_D|\,\sin\left[\phi_{\text{scale}}\,(\phi_D - \phi_A)\right]}{D\,|V_A|} \tag{1}$$

$$\text{TranI} = \frac{|V_A|^2 - |V_D|^2}{|V_A|^2\,D} \tag{2}$$

where

$$D = 1 + 2\frac{|V_D|}{|V_A|}\cos\left[\phi_{\text{scale}}(\phi_D - \phi_A)\right] + \frac{|V_D|^2}{|V_A|^2} \tag{3}$$

with

V_D = voltage output of the! PDP, corresponding to the magnitude of the reflection coefficient, with the dielectric test sample in place

ϕ_D = voltage output of the PDP phase detector, corresponding to the phase of the reflection coefficient. with the dielectric test sample in place

V_A = voltage output of the PDP, corresponding to the magnitude of the reflection coefficient, with the probe tip terminated in air

ϕ_A = voltage output of the PDP phase detector, corresponding to the phase of the reflection coefficient, with the probe tip terminated in air

ϕ_{scale} = an internal calibration factor.

The internal calibration factor, ϕ_{scale}, is determined by comparison of an open circuit measurement (air) to a short circuit measurement obtained by placing a conductive metal across the probe tip:

$$\phi_{\text{scale}} = \frac{180}{\phi_S - \phi_A} \tag{4}$$

where ϕ_S is the voltage output of the PDP phase detector with the probe tip terminated by a short circuit. We use mercury to obtain the short circuit measurement.

The transformation variables, TranR and TranI, are computed separately for the real and imaginary parts of the dielectric constants of the calibration standards, respectively. Figure 9 shows the real and imaginary parts of the calibration

dielectrics plotted against TranR and TranI for one octopus channel. A weighted least squares linear regression is applied to these data to obtain transform equations of the form

$$\epsilon'_r = \epsilon'_{r\text{scale}} \text{TranR} + \alpha' \quad (5)$$

$$\epsilon''_r = \epsilon''_{r\text{scale}} \text{TranI} + \alpha'' \quad (6)$$

for the real (ϵ'_r) and the imaginary (ϵ''_r) parts. The scale factors $\epsilon'_{r\text{scale}}$ and $\epsilon''_{r\text{scale}}$ are given by the slopes of the lines fit to ϵ'_r and ϵ''_r, respectively, and the intercepts α' and α'' approach 1 for ϵ'_r and O for ϵ''_r in the equivalent circuit model.

While in its operational mode, the octopus monitors $|V_D|$ and ϕ_D with the measurement tip as voltage readings that arc stored in the data logger. Prior to beginning each a new measurement sequence for each octopus channel, $|V_A|$ and ϕ_A arc monitored to account for system drifts. Figure 10 shows a 3-day time series of reflection coefficient measurements of the hydroactive xylem tissue of a black spruce tree (*Picea mariana*) at the BCEF. The top graph shows the comparator output voltage, proportional to tile, magnitude and phase of the reflection coefficient as measured in the trunk tissue. The center graph show's these quantities as measured in free space by the reference calibration tip. Applying the calibration actuations to these data yields the tiltle-series dielectric constant shown in the bottom graph.

4 *In situ* Measurement Examples

Several field experiments have been conducted employing our DMS units in concert with systems designed to characterize hydraulic response (water potential)

of vegetation in relation to atmosphere/canopy vapor pressure gradients. Ecophysiological monitoring equipment employed in these studies included xylem sap flow sensors for monitoring water flux in the tree trunks [13] and meteorological sensors for monitoring canopy microclimate. A typical field deployment includes sensors for monitoring xylem dielectric constant, xylem sap flow, photosynthetic active radiation (PAR), air humidity, and temperature of air, woody plant components, and soil at various depths. This section presents a sample of measurements acquired during some field activities. The presentation here is to demonstrate the utility of the dielectric measurement systems in interpreting information concerning plant water status.

4.1 Bonanza Creek Experimental Forest (B CEF), Alaska

During 1993 and 1994, one octopus was deployed within the BCEF, 20 km west of Fairbanks, Alaska, on the Tanana River floodplain. The BCEF is a Long Term Ecological Research site monitored by the U.S. Forest Service and an AIRSAR and ERS-1 study site. We selected two adjacent stands close to an oxbow slough. First, a mature mixed balsam poplar (*Populus balsamifera*) - alder (*Alnus fen uifolia*) stand on a well drained alluvial terrace with gravel and sand deposits. Second, an old white spruce (*Picea glauca*) stand with intermixed black spruce (*Picea mariana*) and alder (*Alnus spec.*) in the understory, growing on a laterally drained soil with permafrost. The rooting system of the balsam poplar stand reaches the ground water' level while the rooting depth in the old w'bite spruce stand is confined to the upper active soil layer where the highest annual soil moisture fluctuations occur.

Annual precipitation is 287 mm. Annual evaporation at the sites in summer ranges from approximately 250 to 330 mm [39].

Fig. 11 shows measurements of the real part of the L-band dielectric constant as measured in the xylem tissue together with the xylem sap flux density for a balsam polar tree and a black spruce tree. Displayed data were acquired between June 24 and July 1, 1993, shortly after the summer solstice. The two trees are separated in the test area by less than 50 meters.

We observed consistently higher xylem flux rates in the balsam poplar tree (top graph) than in the black spruce (bottom graph). At the beginning of the observation period, the xylem dielectric constant of the balsam poplar is significantly higher than that of the black spruce. The balsam poplar dielectric constant decreases over the course of one week until it nearly matches that of the black spruce in terms of absolute magnitude. The week was without rain and high evaporative demand persisted. A decrease in the water content of the poplar may be responsible for the decreasing trend in ϵ_r. In the summer, the black spruce is under moderate but persistent water stress.

From the standpoint of diurnal variation, the balsam poplar exhibits its highest flux rates and xylem dielectric constant between 12:00 and 18:00 and lowest between 00:00 and 06:00. In the case of the black spruce, however, we observe that maxima in both flux and dielectric constant occur between 00:00 and 09:00, while the minima occur between 12:00 and 21:00. One intuitively expects flux maxima to occur mid-day while PAR and vapor pressure difference (VPD) are nigh, and

minima to occur near pre-dawn since these generally represent periods of maximum and minimum evapotranspirative demand, respectively. This is the case with the balsam poplar. However, the black spruce measurements demonstrate that it is possible to have trees with dramatically different flux behaviors even though they are under very similar meteorological conditions. In both trees, we find the diurnal pattern observed in the xylem dielectric constant to be in phase with that of the sap flux.

4.2 BOREAS Field Campaigns, Canada

The Boreal Ecosystem - Atmosphere Study (BOREAS) is a multidisciplinary field and remote sensing study the goal of which is to obtain an improved understanding of the interactions between the boreal forest biome and the atmosphere in order to clarify their roles in global change. The two principal BOREAS field sites, both located within Canada, are located in the southern boreal ecotone, encompassing Prince Albert National Park, Saskatchewan, and in the northern boreal ecotone near Thompson, Manitoba. During 1994, we instrumented a total of four stands at the northern and southern BOREAS test sites (designated NSA and SSA, respectively) with an entire suite of sensors which operated throughout much of the growing season [22, 47]. An L-band octopus was installed at the SSA young jack pine (YJP) stand and individual single channel DMS units were installed at the SSA old jack pine (OJP) stand (P-band), SSA old black spruce (OBS) stand (P-band), ant{ NSA old black spruce (OBS) stand (C-band).

Fig. 12 includes several graphs that summarize measurements of xylem dielec-

tric constant and sap flux in three individual trees, one in each of stands SSA OJP, SSA OBS, and NSA OBS. Dielectric constant is plotted for April 24-30 and June 5-11, 1994 and xylem flux density is plotted for June ,5-11. All three trees exhibit sonic diurnal variation in their xylem dielectric constant with a pronounced stand-to-stand variation. The change in diurnal response in dielectric constant from April to June is also notable. The SSA OJP tree shows similar amplitude variation during both April and June, but the maxima are inverted. During April, ϵ_r reaches minimum values at the end of the night while in June the lowest ϵ_r occurs during late afternoon when the stem water storage is depleted and water potential is lowest. The dielectric of the NSA OBS tree shows a marked increase from April to June in both its absolute level and in its magnitude of diurnal fluctuation. The xylem dielectric constant of tile SSA OBS tree flattens to a nearly constant value of approximately *10* as the growing season progresses into June. It is also noteworthy that the xylem flux rate in this black spruce tree is very low. Xylem sap flux behavior is similar for all three trees, with SSA OJP showing the largest and SSA OBS showing smallest daytime magnitudes.

Fig. 13 shows xylem sap flux, vapor pressure deficit, air and soil temperature, and xylem dielectric constant (C-band) for a single tree in the NSA OBS stand from April 10 (DOY 100) through November 6, 1994 (DOY 310). This period spanned the entire growing season. Although the dielectric constant measurement series was begun after the tree trunks began to thaw, a notable increase in absolute level of ϵ_r occurred between DOY 125 and DOY 130 (May 5-1 O). This corresponds

to the period during which the upper 40 cm of the soil and moss layer thawed, thus allowing the plant to draw more water from the soil. As the growing season progresses into late summer and fall, a decrease in the amplitude of the diurnal variations in xylem dielectric constant and also a general decrease in its absolute magnitude was observed. Freeze-up occurred in late October.

Fig. 14 shows, for the SSA YJP stand, PAR, air temperature and VPD, xylem flux density, mean xylem dielectric constant of eight jack pine trees (L-band, real part), and xylem dielectric constant of four selected individuals during a three clay period from July 22-24, 1994. For each individual tree, xylem dielectric constant was measured with a single coaxial probe inserted to a depth between 0..5 and 1.5 cm within the hydroactive xylem tissue of the main stem. Absolute values of mean dielectric constant were generally low and increased by about 25% from daytime to nighttime. Lowest values were observed from midday through late evening with highest values occurring briefly past midnight through sunrise. Mean xylem dielectric constant showed a decrease with higher VPD and sap flux density but the trend was not significant. Individual trees varied widely in trend and diurnal amplitude of xylem dielectric constant changes (Fig. 14, bottom). Maximum increase observed in a single individual was approximately 60% diurnally, while in some other individuals almost no diurnal variation was observed. The variability was not explained by variation in tree size or relative canopy exposition and was not correlated with measured water potential changes. In individual trees, the correlation between xylem dielectric constant, micro-r meteorological parameters,

tree water status and xylem flux density was weak.

4.3 Gippsland Eucalyptus Forest, Victoria, Australia

One particularly interesting example of a tree's dielectric response to meteorological parameters was observed during the 1993 NASA/JPL AIRSAR deployment to Australia. During this deployment, we installed three single channel DMS units in the Gippsland region of Victoria, Australia. This region contains an area of native forests in the foothills of the Great Dividing Range [1, 10]. The two dominant species of these forests are white stringy bark (Eucalyptus *globoidea*) and red box (*Eucalyptus polathemos*), whose populations are 60% and 30%, respectively. These species are intermixed with mountain grey gum (*Eucalyptus cypellocarpa*), reel ironbark (*Eucalyptus sideroxylon*), candlebark (*Eucalyptus rubida*), and silver wattle (*Acacia dealbata*). In this study, we examined the trees' diurnal dielectric response and determine the sensitivity of radar backscatter to diurnal changes in dielectric constant. Although several rain showers impaired the interpretation of AIRSAR backscatter data, the significant input of rain water did lead to some interesting dielectric observations.

Fig. 15 shows the P-band dielectric response measured in the trunk of a white stringybark over several clays during September, 1993. From September 5 - 7, dielectric constant reached maximum values at about 10:00 each morning. Between 11:00 and 13:00, a marked decrease in dielectric constant occurred during each of these clays. The maximum such decrease occurred on Sept. 7 when the real part of ϵ_r dropped from a value of 15 to a minimum of 7, a decrease of more than 50%.

This decrease coincides with the period of increasing evapotranspirative demand on the tree. Dielectric remained relatively low between 13:00 and 19:00, when recovery began. During this time, the loss tangent varied from a maximum of 0.36 in the mornings to a minimum of 0.15 after midday.

A light rain began falling during the morning of September S, with moderate rain showers beginning mid-afternoon. Records from a weather station in Mafra, several kilometers away, indicated that 22.2 mm of rain fell during the 24 hours following 9:00 September 8. Up to that time, this was one of the largest rain events recorded in Mafra during 1993. An additional 4.6 mm then fell on Sept. 9 after midday.

The effect of this large influx of water on the dielectric constant is dramatic. Whereas the diurnal trend in ϵ_r continued through Sept. S, an increasing trend in dielectric began on the morning of Sept. 9. The timing of this increase coincides with the mid-morning increase in evapotranspirative demand. The increase in dielectric continues through midday Sept. 12 when the more familiar diurnal pattern returns.

Another 12.6 mm of rain fell on Sept. 12., as measured at the weather station in Mafra. This rain event is again reflected as an increase in ϵ_r beginning with the mid-morning increase in evapotranspirative demand On that day. The measurement series ends on Sept. 13 with ϵ_r approaching $28 - j\ 19$.

The loss tangent increased from about 0.2011 Sept. S, to about 0.7 late night Sept. 11, thus reflecting the increase in ϵ_r'' relative to ϵ_r'. As ϵ_r'' is more sensitive to

changes in ionic concentration than is ϵ'_r, it is likely that the observed trend in loss tangent reflects a change in xylem fluid chemistry that occurred as a result of the large influx of water into the rooting zone and then into the xylem tissue brought about by the rain events.

5 Concluding Remarks

Continuous monitoring of vegetation dielectric properties promotes understanding of the variations in dielectric constant that occur on both seasonal and short-term (diurnal) time scales. We have presented the design and implementation of a dielectric measurement system (DMS) that allows automated and continuous *in situ* monitoring of the dielectric behavior of woody vegetation tissue. Implementation of both single channel and multi-channel (octopus) systems were discussed. These systems employ the same measurement technique as the Portable Dielectric Probe built by Applied Microwave Corporation but have been adapted to facilitate the continuous and long-term monitoring of vegetation canopy dielectric behavior in remote field sites.

We presented a sample of *in situ* data obtained from a series of three field studies during which we deployed several of these systems. These examples demonstrate that together with contemporaneous hydraulic and meteorological measurements, measurements obtained with our systems give new insight into the dielectric behavior of vegetation with respect to physiological and hydraulic function. The interpretation of tile temporal response of vegetation dielectric constant and its

relationship to physiological and hydraulic parameters should prove most useful in linking these parameters to radar remote sensing observations.

Acknowledgments

The authors gratefully acknowledge the helpful technical advice received from Craig Dobson at The University of Michigan and David Brunfeldt at Applied Microwave Corporation. We thank the following collaborators for their assistance with obtaining the *in situ* measurements: Prof. Ram Oren (Duke University, Durham, North Carolina); Dr. Cynthia Williams, Dr. Leslie Viereck and Mr. Andrew Balser (Institute of Northern Forestry, Fairbanks, Alaska); Prof. Tony Milne, Dr. Yunhan Dong, and Mr. Ed Knowles (University of New South Wales, Australia). We also thank Abel Guerra for construction of an early prototype of the multiplexing unit.

'l'his work was carried out at the Jet I'repulsion Laboratory, California Institute of Technology, under contract to the National Aeronautics and Space Administration. BOREAS is co-sponsored by the National Aeronautics and Space Administration and Energy, Mines and Resources, Canada.

References

[1] Ahmed, z., "Radar backscatter modelling of forested regions containing arbitrarily oriented woody structures," Ph.D. dissertation, The [University of New South Wales, Sydney, .Australia, 1991, pp. 54-55.

[2] Applied Microwave Corporation, Manual for Portable Dielectric Probe, Applied Microwave Corporation, Lawrence, Kansas, 1989.

[3] Bonan, G. R., "Atmosphere-biospheree xchangcclof carbon dioxide in boreal forest s," *JotLrrlalo fGeoptLysicall te.scale/L,vol.96,* pp. 7301-7312,1991.

[4] Brunfeldt, D. R., "Theory and Design of a Field-Portable Dielectric Measurement System, " *Proc.of the 1987 International Geoscience and Remote Sensing Symposium* Ann Arbor, Michigan, May 18-21, pp. 559-563.

[5] Chauhan, N. S., R, H. Lang and K. J. Ranson, "Radar modeling of a boreal forest ," *IEEE Transactions on Geoscience and Remote Sensing, vol.* GE-29, pp. 627--63S, 1991.

[6] Dickinson, R. E., A. Ilenclmson-Sellers, P. J. Kennedy and M. F. Wilson, "Biosphere-Atmosphere 'Transfer Scheme (BATS) for the NCAR Community Climate Model, " NCAR Technical Note NCAR/TN-275+STR, National Center for Atmospheric Research, December 19S6.

[7] Dobson, M. C., "calibration of field portable dielectric I'robes for use in radar experiments, " Radiation Laboratory '1'ethnical Report, The University of Michigan, Ann Arbor, May 1990.

[8] 1)0}) s011, M. **c.,** "Diurnal and seasonal Variations in the Microwave Dielectric Constant of Selected Trees," *Proceedings of International Geoscience and Remote Sensing Symposium,* 12-16 September 19SS, Edinburgh, U.K., Vol. 3, p. 1754.

[9] Dobson, M. C., R. de la Sierra and N. Christensen, "Spatial and Temporal Variation of the Microwave Dielectric Properties of Loblolly Pine Trunks," *Proceedings of International Geoscience and Remote Sensing Symposium,* 3-6 June 1991, Espoo, Finland.

[10] Dong, Y., "A long wavelength radar backscatter model for forests." Ph. D. dissertation, The University of New South Wales, Sydney, Australia, 1995, pp. 130-132.

[11] Durden, S. L., J. J. van Zyl and [1. A. Zebker, "Modeling and observation of' the radar polarization signature of forested areas, " *IEEE Transactions on Geoscience and Remote Sensing,* vol. 27, *110. 3,* May 19s9, pp. 290-:301.

[12] El-Rayes, M. A. and F. T. Ulaby, "Microwave dielectric spectrum of vegetation, Part 1: Experimental observations, " *IEEE Transactions on Geoscience c2nd Remote Sensing,* vol. GE-25, no. 5, September 1987.

[13] Granier, A., " Evaluation of Transpiration in a Douglas-fir Stand by means of Sap Flow Measurements," *Tree Physiology* Vol. 3, 19S7, pp. 309--319.

[14] Harbinson, J. and F. I. Woodward, "The use of microwaves to monitor the freezing and thawing of water in plants," *Journal of Experimental Botany,* vol. 38, pp. 1325-1335, 19s7.

[15] Holbrook, N. M., M. J. Burns and '1'. R. Sinclair, "Frequency and Time-Domain Dielectric Measurements of Stem Water Content in the arborescent palm, *Sabal palmetto," Journal of Experimental Botany, vol. 43,* 110.246, *pp.* 111-119, January 1992.

[16] Karam, M. A. and A. K. Fung, "Electromagnetic scattering from a layer of finite length randomly oriented dielectric circular cylinders over a rough interface with application to vegetation, " *International Journal of Remote Sensing,* vol. 9, no. 6, June 1988, pp. 11091134.

[17] Lang, R. 11., N. S. Chauhan, K. J. Ranson and O. Kilic, "Modelling P-band SAR returns from a red pine stand," *Remet e Sensing of Environ ment,* vol. *47,* pp.132-141, 1994.

[18] McDonald, K. C. and W. Chun, Inventors, "Automated monitoring of dielectric properties of tree trunks," *NASA* Tech *Briefs,* vol. 20, no. 3, March 1996, pp. *44-46.*

[19] McDonald, K. C. and W. Chun, "Dielectric Monitoring System," JPL Notice of New Technology, Item No. S929, 1993.

[20] McDonald, K. C., M. **C.** Dobson and F. T. Ulaby, "Using MIMICS to model I.-band multi-angle and multi-temporal backscatter from a walnut orchard," *IEEE Transactions on Geoscience and Remote Sensing,* vol. 2S, no. 4, 1990, pp.477-491.

[21] McDonald, K. C., M. C. Dobson and F. 1'. Ulaby, "Modeling multifrequency diurnal backscatter from a walnut orchard," *IEEE Transactions on Geoscience and Remote Sensing,* vol. 29, no. *6,* 1991, pp. 852-863.

[22] McDonald, K. C. R. Zimmermann, R. Oren and J. B. Way, "Dielectric and hydraulic response of selected forest canopies at the BOREAS test sites in Canada," *Proc. of the 1995 International Geoscience and Remote Sensing Symposium*, Fierenze, Italy.

[23] Morgan, M. T., R. K. Wood and R. G. Holmes, "Dielectric moisture measurement of soil cores," 1991 *International Winter Meeting of the American Society of Agricultural Engineers*, Chicago, Illinois.

[24] Nobel, P. S., Biophysical plant physiology and ecology, W. H. Freeman and Co. San Francisco, 1983, pp.608

[25] Oren, R., R. Zimmermann and J. Terborgh, "Transpiration in upper Amazonia floodplain and upland forests in response to drought breaking rains," Ecology. vol. '77, no. 3, 1996, pp. 96 S-973

[26] Page, J., Planet Earth: Forest, T. A. Lewis, Editor, Time-Life Books, Inc., p. 81, 19s3.

[27] Pissis, P., A. Anagnostopoulou-Konsta and L. Apekis, "A dielectric study of the state of water in plant steins," *Journal of Experimental Botany*, vol. 38, pp. *1.528-1.540*, 1987.

[28] Richards, J. A., "Radar backscattering of forests: A review of current trends," *International Journal of Remote Sensing*, vol. 11, no. 7, pp. 1299--1312, 1990.

[29] Rignot, E., and J. B. Way, "Monitoring freeze-thaw cycles along north-south Alaskan transects using ERS-1 SAR," *Remote Sensing of Environment*, vol. 49, pp. 131-137, 1994.

[30] Romberger, J. A., Z. Hejnowicz, J. F. Hill, Plant Structure: Function and Development, Springer Verlag, Berlin, 1993, pp.524

[31] Salas, W. A, K. J. Ranson, B. N. Rock and K. T. Smith, "Temporal and spatial variations in dielectric constant and water status of dominant forest species from New England," *Remote Sensing of Environment*, vol. *47*, pp. 109--119, 1994.

[32] Stuchly, M. A., and S. S. Stuchly, "Coaxial line reflection methods for measuring dielectric properties of biological substances at radio and microwave frequencies - A Review," *IEEE Transactions on Instrumentation and Measurement, vol.* IM-29, *no.* 3, pp. 176- 1S3, September 19S0.

[33] Sun, G. and D. S. Simonette, "A composite L-band HH radar backscattering model for coniferous forest stands", *Photogrammetric Engineering and Remote Sensing,* vol. 54, 110.s, pp. 1195-1201, 1988.

[34] Tan, 11. S.," Microwave measurements and modeling of the permittivity of tropical vegetation samples," *Applied Physics,* vol. 25, pp. 351-355, 1981.

[35] Tsang, L. and J. Kong, "Application of strong fluctuation random medium theory to scattering from vegetation-like half space," *IEEE Transactions on Geoscience and Remote Sensing, vol.* 19, no. 1, 1981, pp. 62-69.

[36] Ulaby, F. T., ant{ h]. A. El-Rayes, "Microwave dielectric spectrum of vegetation, Part II: Dual-dispersion model, " *IEEE Transactions of Geoscience and Remote Sensing, vol.* GE-25, pp. *.550 -5.5'7, 19S7.*

[37] Ulaby, F'. 1., R. K. Moore and A . K. Fung, Microwave Remote Sensing, Active and Passive, Appendix E, Dedham, MA: Artec House, 19S6

[3S] Ulaby, F. T., K. Sarabandi, K. McDonald, M. Whitt and M. C. Dobson, "Michigan Microwave Canopy Scattering Model (MIMICS) ," *International Journal of Remote Sensing,* vol. 11, no. 'i', 1990, pp. 1223-1253.

[39] Viereck I,.. A., K. Van Cleve, P. C. Adams and R. E. Schlentner, "Climate of the Tanana River floodplain near Fairbanks, Alaska," *Canadian Journal of Forest Research, vol.* 23, 1993, pp. 89!+!313.

[40] Waring, R. 11., and W. 11. Schlesinger Forest Ecosystems: Concepts and Management, Academic Press, inc., Orlando, Florida, 1985, pp. 340.

[41] Way, J. B., K. McDonald, E. Paylor, G. Karas, S. Chernobieff and N. Biery, "Collected data of the Bonanza Creek Experimental Forest, Alaska, Volume 1: AIRSAR ancl In Situ Measurements, March 198 S," CD ROM, The Jet Propulsion Laboratory, 1992.

[42] Way, J.B. J. Paris, M. C. Dobson, K. C. McDonald, F. T. Ulaby, J. A. Weber, S. I,. Ustin, V. C. Vanderbilt and E. S. Kasischke, "Diurnal change in trees as observed by optical and microwave sensors: The EOS synergism study," *IEEE Transactions on Geoscience and Remote Sensing,* vol. 29, no. 6, 1991, pp. 807-821.

[43] Way, J. 11.,,1. Paris, E. Kasischke, C. Slaughter, I.. Viereck, N. Christensen, M. C. Dobson, 1'.1'. Ulaby, J. Richards, A. Milne, A. Sieber, F'. J. Ahern, D.

Simonett, R. Hoffer, M. Imhoff and J. Weber, "The effect. of changing environmental conditions on microwave signatures of forest ecosystems: Preliminary results of the March 1988 Alaskan aircraft SAR experiment, " *International Journal of Remote Sensing,* vol. 11, pp. 1119--1144, 1990.

[44] Way, J. B., E. Rignot, K. C. McDonald, R. Oren, R. Kwok, G. Bonan, M. C. Dobson, L. A. Viereck and J. E. Roth, "Evaluating the type and state of Alaska tiaga forests with imaging radar for use in ecosystem flux models," *IEEE Transactions on Geoscience and Remote Sensing,* vol. 32, no. 2, pp. 353-370, 1994.

[45] Way, J.B., R. Zimmermann, E. Rignot and K. McDonald, "Winter and spring thaw as observed with imaging radar at I1OREAS," *Journal of Geophysical Research,* Accepted.

[46] Weber, J. A. and S. I,. Ustin, "Diurnal Water Relations of Walnut Trees: Implications for Remote Sensing," *IEEE Transactions on Geoscience and Remote Sensing,* vol. 29, no. 6, pp. 864-874, Nov. 1991.

[47] Zimmermann, R., K. C. McDonald, R. Oren and J. B. Way, "Xylem dielectric constant, water status, ant{ transpiration of young Jack Pine (Pinus banksiana Lamb.) in the southern boreal zone of Canada," *Proc. of the 1995 International Geoscience and Remote Sensing Symposium,* Fierenze, Italy.

Figure 1: [Illustration of the anatomy of a tree bole showing the bark, bast, bast cambium, phloem and xylem regions.
from Planet Earth: Forest,
Art by Trudy Nicholson,
©1983 Time-Life Books Inc. [26]

Figure 2: System- 1evel block diagram of the Applied Microwave Corporation Field Portable Dielectric Probe (PDP).

Figure 3: Dielectric constant as a function of depth into a white spruce tree bole. Data shown are 1,-band (1.2 GHz) measurements obtained during the March 19SS JPL AIRSAR deployment to the Bonanza Creek Experimental Forest, Alaska.

Figure 4: System-1evel block diagram of the single-channel dielectric monitoring system incorporating a single PDP with a custom-built switching assembly and a Delta-T Devices data logger.

Figure 5: System-level block diagram of a multi-channel dielectric monitoring system, incorporating a single PDP with a custom-built multiplexing unit, several measurement/calibration switch assemblies, and a Delta-T Devices data logger. The system shown in this diagram allows multiplexing of four independent channels with a single PDP. The systems thus far deployed allow multiplexing of up to eight independent channels and thus each is referred to as an '(octopus>'. Additional PDPs of different operating frequencies can be multiplexed at the input to the microwave switching network, allowing multifrequency measurements to be made with a single installation.

Figure 6: Photograph of an eight channel multiplexing unit and one measurement/calibration switch assembly. The series of cables and connectors across the bottom of the multiplexing unit arc the eight switch control cables that control switching of the measurement/calibration switch assemblies. 'I'he two sets of eight SMA-type connectors above them connect to the eight measurement/reference cable pairs. The two SMA-type connectors 011 the extreme right hand side interface with the PDP comparator circuitry. The two coaxial probes connected to the measurement calibration switch assembly arc the reference calibration and measurement probes.

Figure 7: Installation of a measurement/calibration switch assembly on a balsam poplar tree. (a) The assembly is strapped to tile tree with the measurement tip implanted in the hydroactive tissue of the tree trunk. (b) The measurement and switch control cables and the reference calibration tip are attached to the assembly. As shown, the reference calibration tip is suspended in an air-tight vial that contains some desiccant so moisture does not condense on the reference tip.

Figure S: For long-term installation of the octopus, the measurement/reference cable pairs are run through protective PVC pipes. 'l'his photograph is of a test site in the Bonanza Creek Experimental Forest, Alaska, on the Tanana River floodplain where several individual trees have been instrumented with a single octopus. The switch assemblies installed on the trees have been covered with insulation for protection from direct exposure to rain and snow.

Figure 9: Graph of dielectric constant vs. transform variable used in determining the transform from the measured reflection coefficient, to the dielectric constant. The transformations for both the real and the imaginary parts of the dielectric constant are shown on this plot. The relationships shown here have been derived from measurements of air, amyl alcohol, hexyl alcohol, ethylene glycol, 1 -propanol, 1- butanol, and methanol.

Figure] 0: Time series plot recorded during July, 1993, showing: (top) magnitude and phase of reflection coefficient measured in the hydroactive xylem tissue of a black spruce tree, (center) corresponding magnitude and phase of reflection coefficient measured with the calibration reference tip in air, and (bottom) dielectric constant computed from the reflection coefficient measurements.

Figure 11: Xylem dielectric constant (1,-band, real part) and xylem sap flux (grams H_2O/m^2 sec.) as measured for a balsam poplar (top) and a black spruce (bottom). These data were obtained during 1993 at the Bonanza Creek Experimental Forest, Alaska, along the Tanana River floodplain between June 24 (DOY 175) and July 1 (DOY 1S2). Numerical labels on the horizontal axis indicate midnight on that respective day.

Figure 12: Xylem dielectric constant (real part) and xylem sap flux density (in grams/m^2sec.) as observed in the SSA Old Jack Pine (P-band), NSA Old Black Spruce (C-band), and SSA Old Black Spruce (C-band) stands at BOREAS during 1994. The dielectric constant is shown for April 24-30 and June 5-11. Xylem flux density is shown for June .5-11.

Figure 13: Data series recorded for the Old Black Spruce stand at the BOREAS Northern Study Area for the duration of the 1994 growing season. In order from top to bottom: Xylem sap flux, vapor pressure deficit (VPD), air temperature, soil temperature at three depths between O and 40 cm, trunk xylem tissue temperature, and xylem dielectric constant (C-band). Dielectric data between DOY 163 and DOY 200 is missing because of damage to system cables by wildlife. Xylem flux measurements prior to DOY 138 and after DOY 268 have not been fully interpreted because of ambiguities caused by the freeze/thaw transition periods.

Figure 14: Photosynthetic active radiation (top), mid-canopy air temperature and vapor pressure deficit (second from top), xylem sap flux density (third from top), mean xylem dielectric constant (1,- band, real part) of eight trees (second from bottom, error bars indicate standard error), and xylem dielectric constant of four selected individuals of jack pine (*Pinus banksiana*) *in* a young uniform stand for three clays (July 22-24, 1994) at the BOREAS Southern Study Area.

Figure 1.5: P-band (0.45 GHz) dielectric response of a white stringy bark as measured from 12:00 noon, Sept. 4 through 12:00 noon Sept. 13. Numerical labels on the horizontal axis indicate midnight on that respective day. Real and imaginary parts of the dielectric constant are shown together with the loss tangent. Rain showers began on September S.

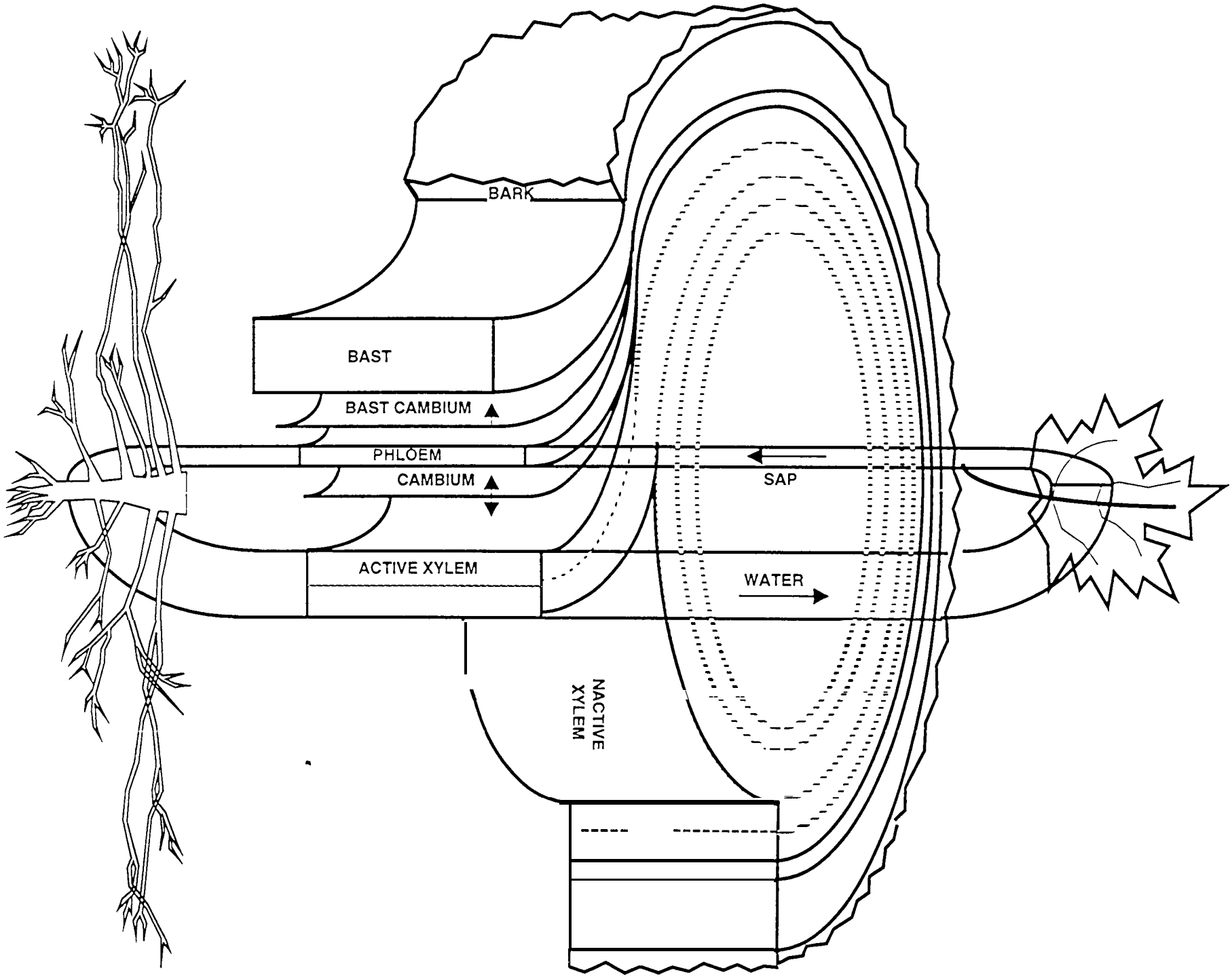
BARK
BAST
BAST CAMBIUM
PHLOEM
CAMBIUM
SAP
ACTIVE XYLEM
WATER
NACTIVE XYLEM

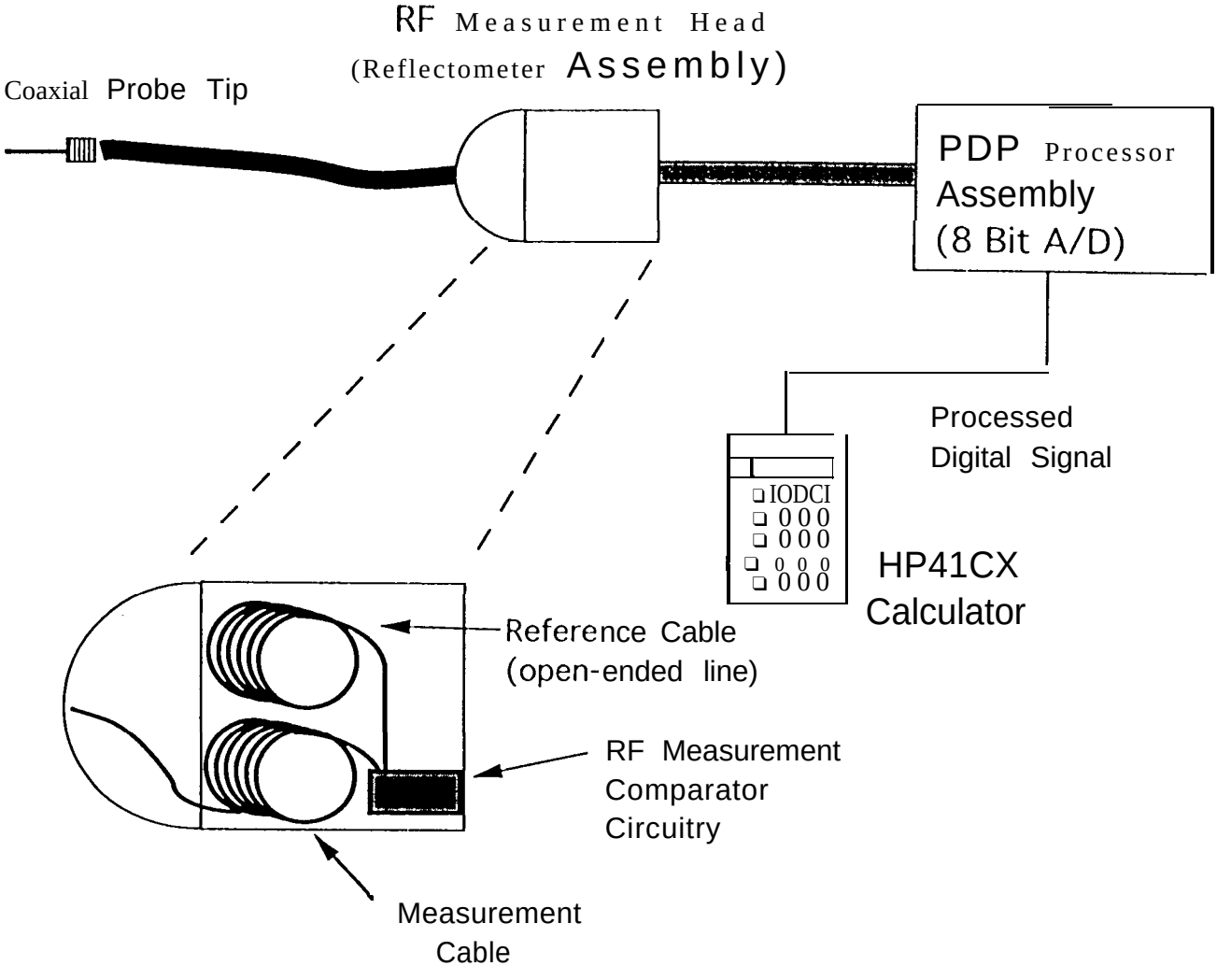
RF Measurement Head
(Reflectometer Assembly)
Coaxial Probe Tip
PDP Processor
Assembly
(8 Bit A/D)
Processed
Digital Signal
IODCI
HP41CX
Calculator
Reference Cable
(open-ended line)
RF Measurement
Comparator
Circuitry
Measurement
Cable

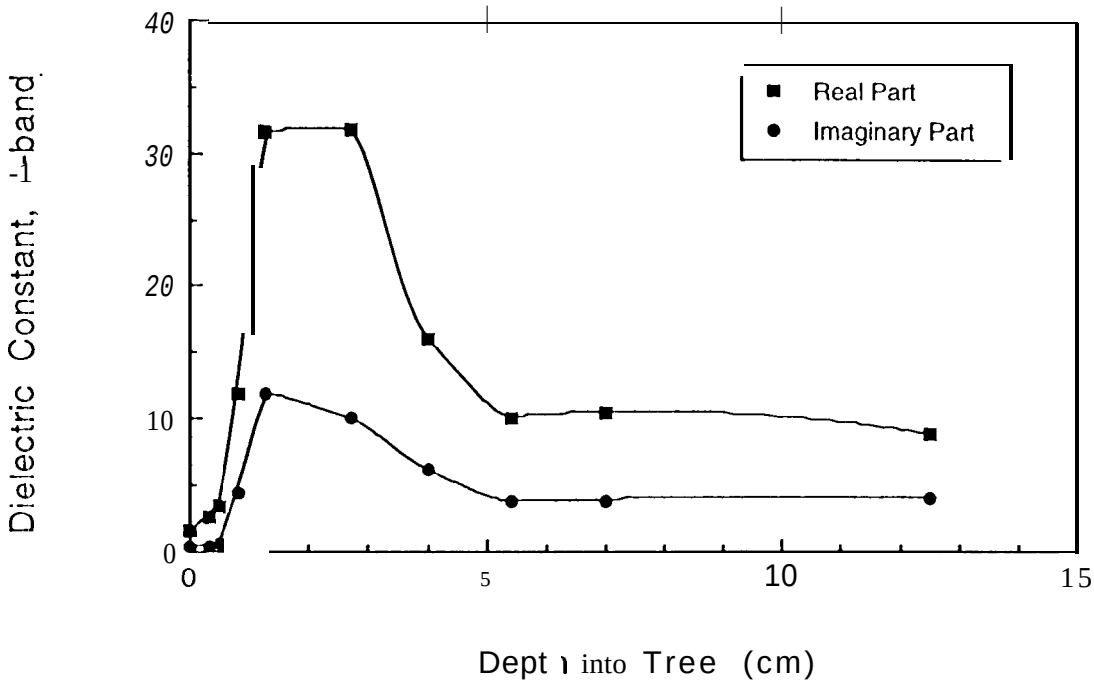
Dielectric Constant, L-band
40
30
20
10
0
0
5
10
15
Real Part
Imaginary Part
Dept ı into Tree (cm)

Fig 3

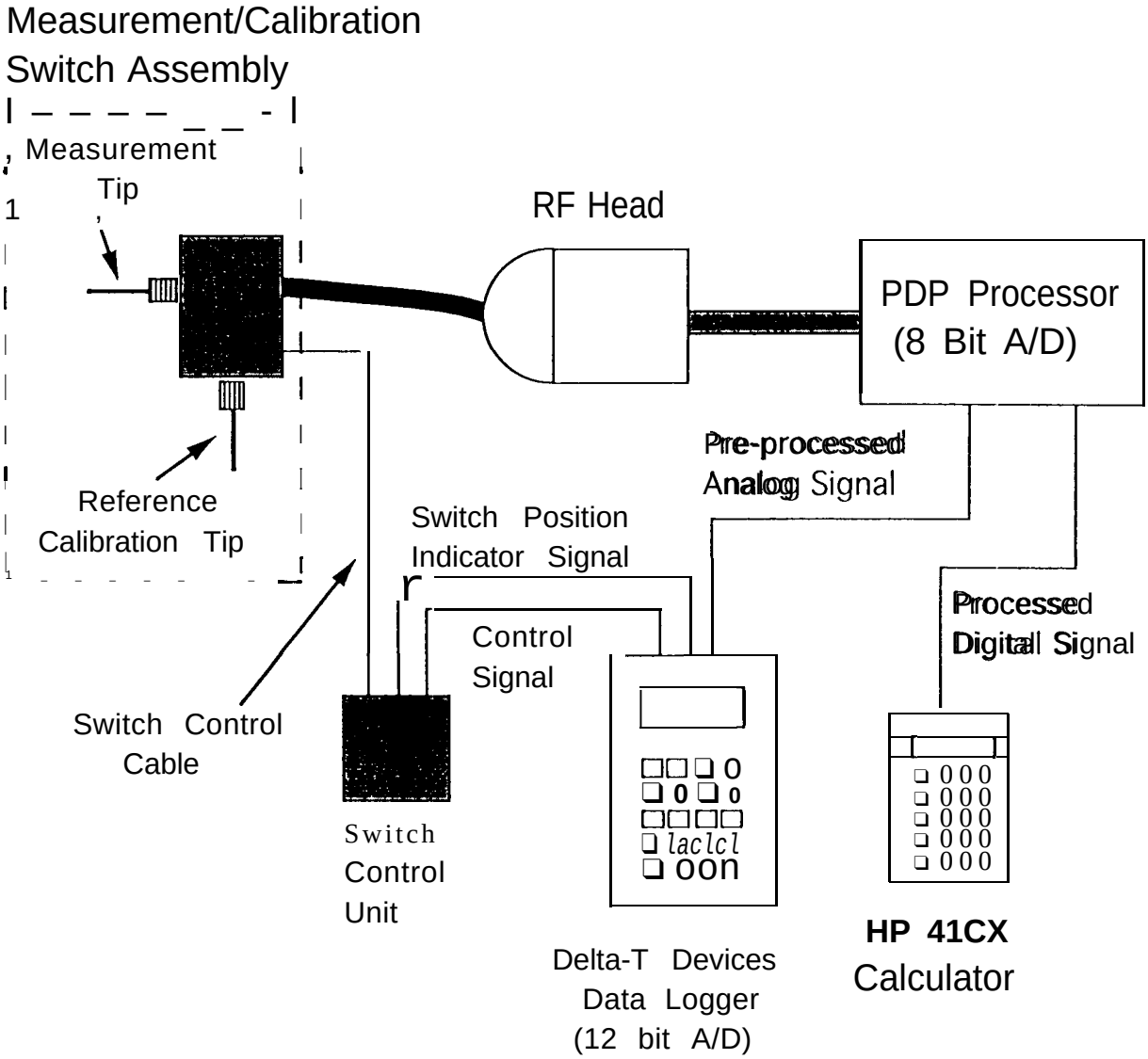
Measurement/Calibration
Switch Assembly
Measurement
Tip
RF Head
PDP Processor
(8 Bit A/D)
Pre-processed
Analog Signal
Reference
Calibration Tip
Switch Position
Indicator Signal
Control
Signal
Processed
Digital Signal
Switch Control
Cable
Switch
Control
Unit
Delta-T Devices
Data Logger
(12 bit A/D)
HP 41CX
Calculator

Fig 4

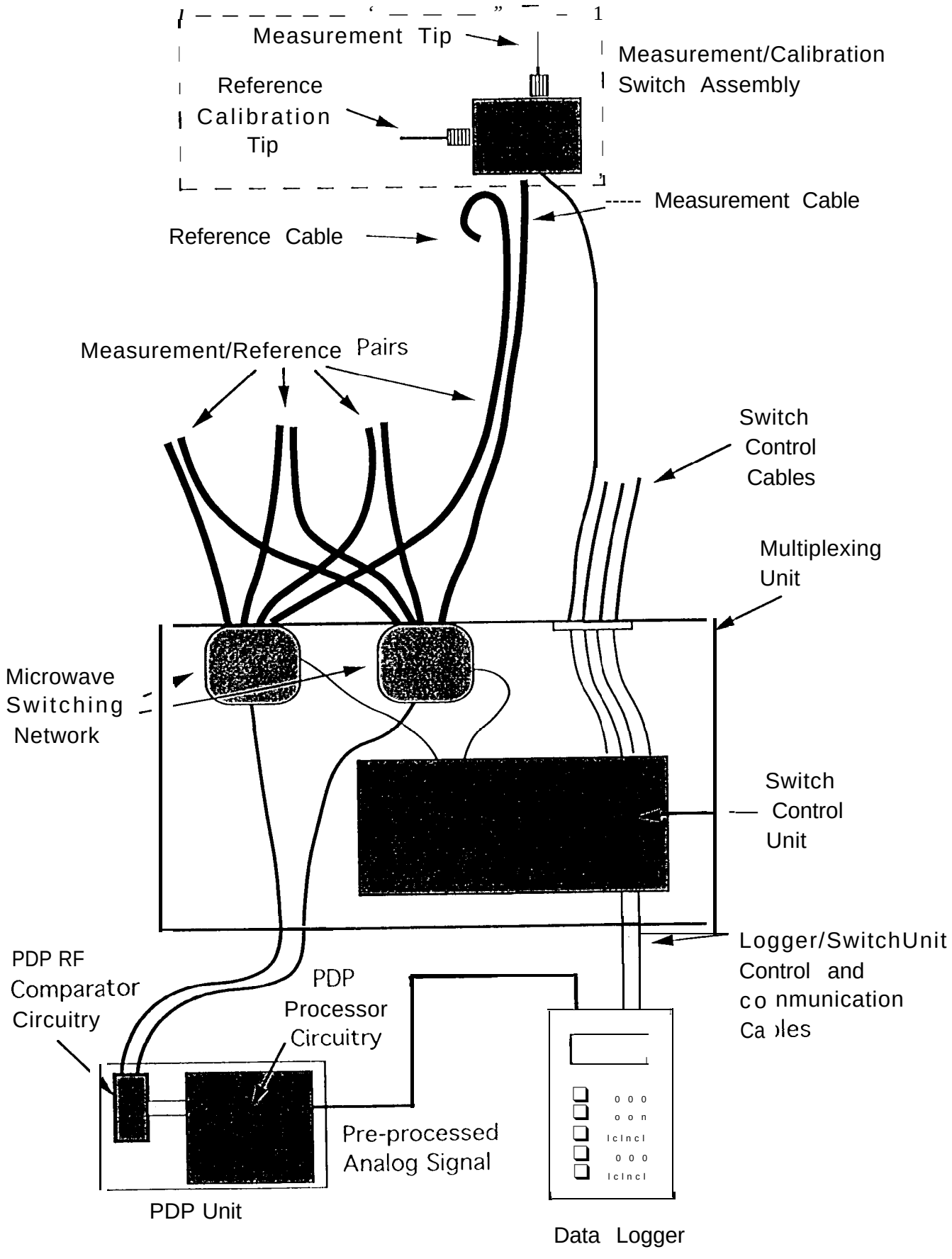
Measurement Tip
Measurement/Calibration
Switch Assembly
Reference
Calibration
Tip
Measurement Cable
Reference Cable
Measurement/Reference Pairs
Switch
Control
Cables
Multiplexing
Unit
Microwave
Switching
Network
Switch
Control
Unit
Logger/SwitchUnit
Control and
co nmunication
Ca)les
PDP RF
Comparator
Circuitry
PDP
Processor
Circuitry
Pre-processed
Analog Signal
PDP Unit
Data Logger

Fig 5

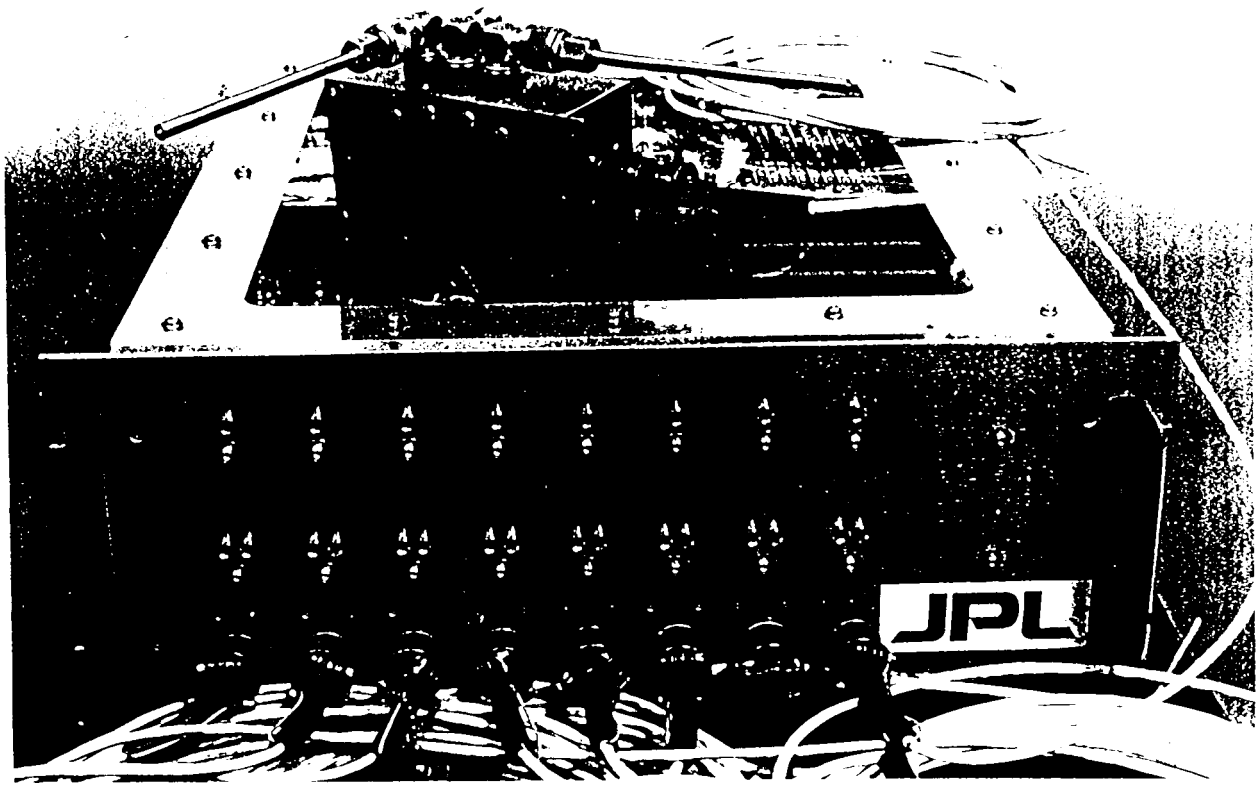

Fig 6

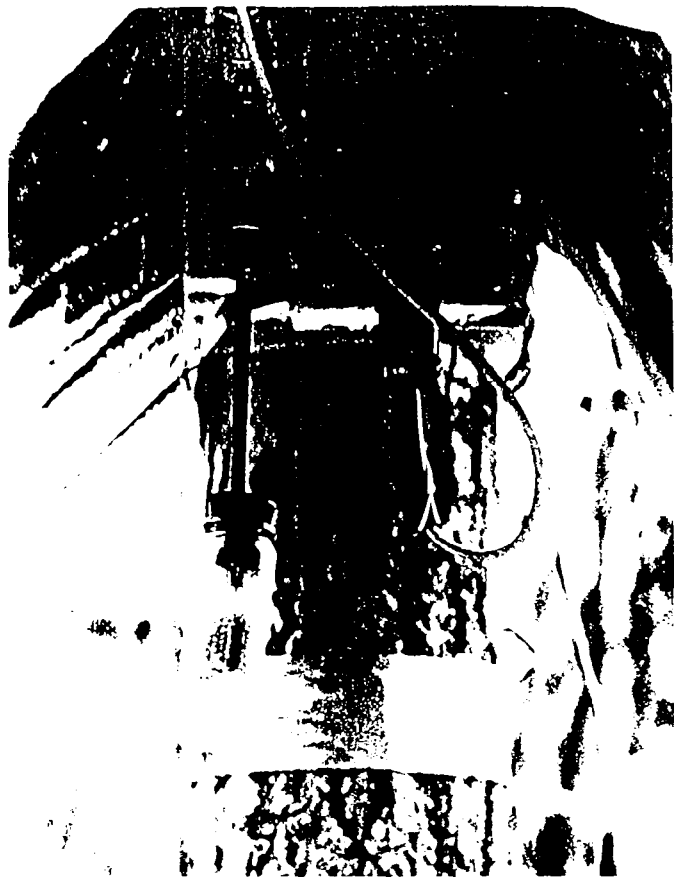

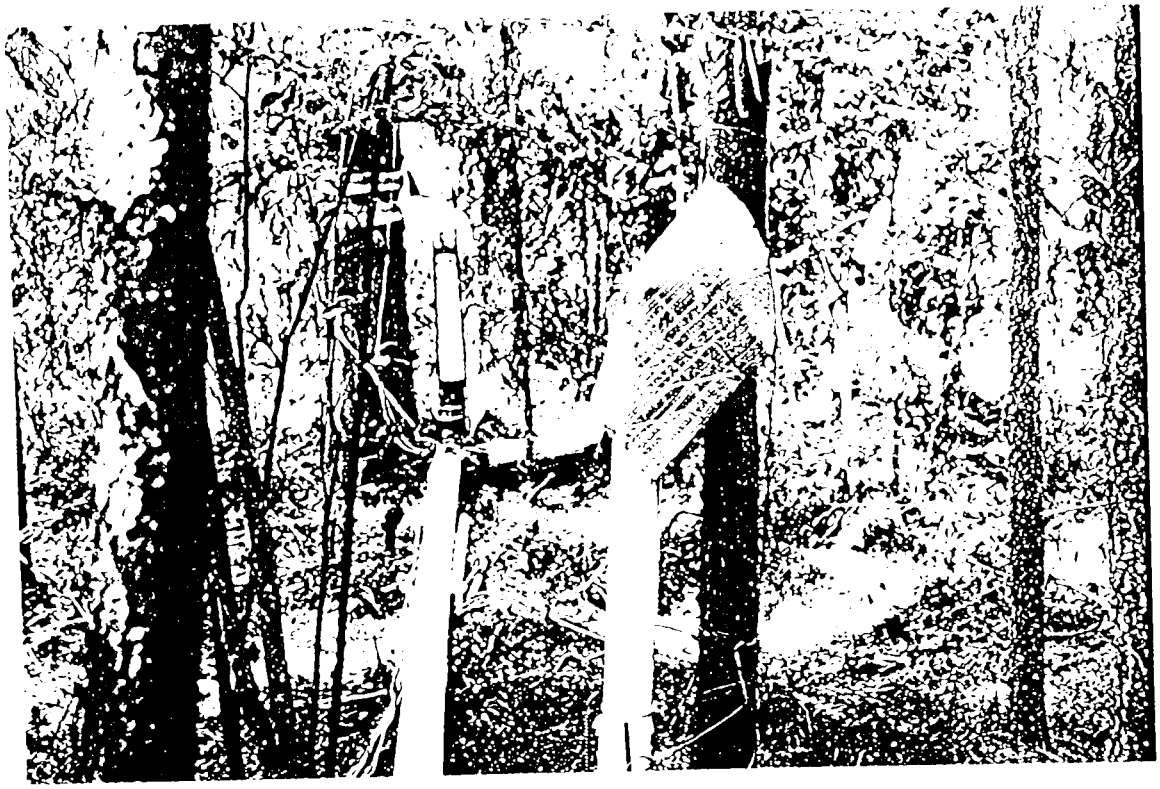

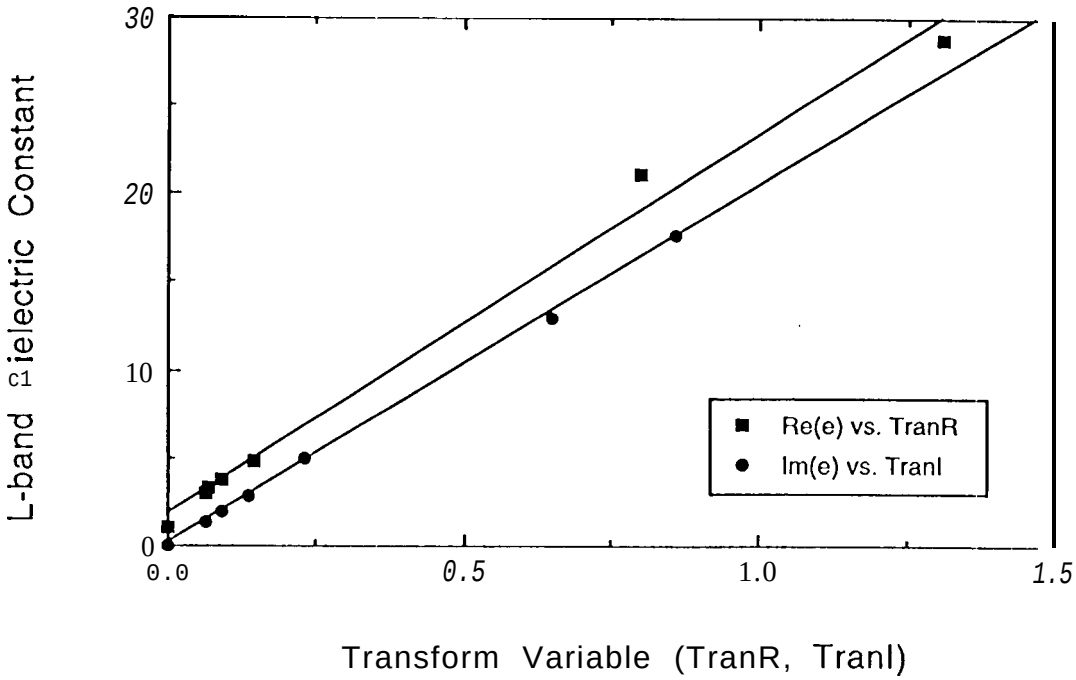
30
20
10
0
0.0
0.5
1.0
1.5
L-band Dielectric Constant
Re(e) vs. TranR
Im(e) vs. TranI
Transform Variable (TranR, TranI)

Fig 9

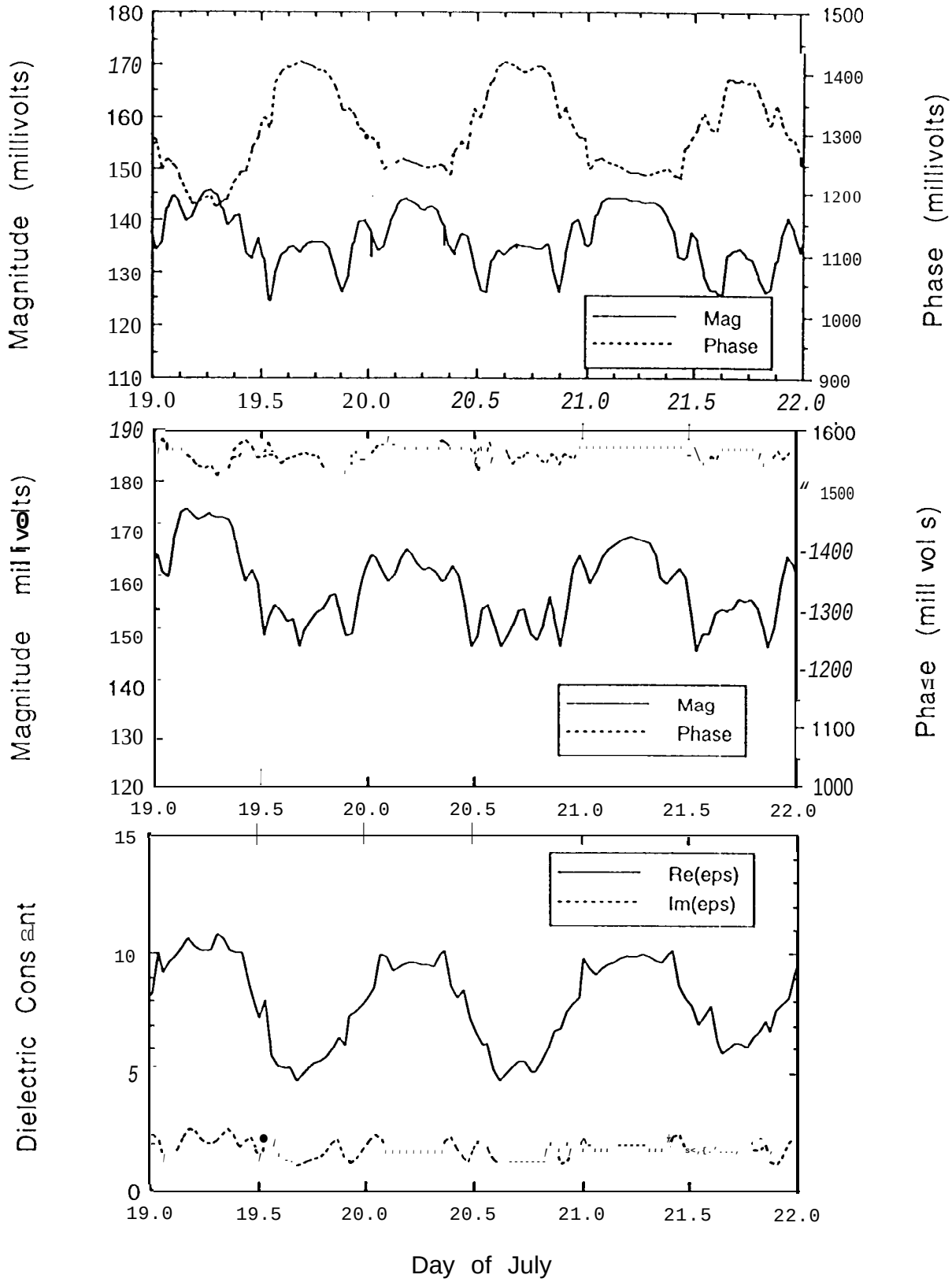
Magnitude (millivolts)
Phase (millivolts)
Mag
Phase
Magnitude mil volts)
Phase (mill vol s)
Mag
Phase
Dielectric Constant
Re(eps)
Im(eps)
Day of July

Fig 10

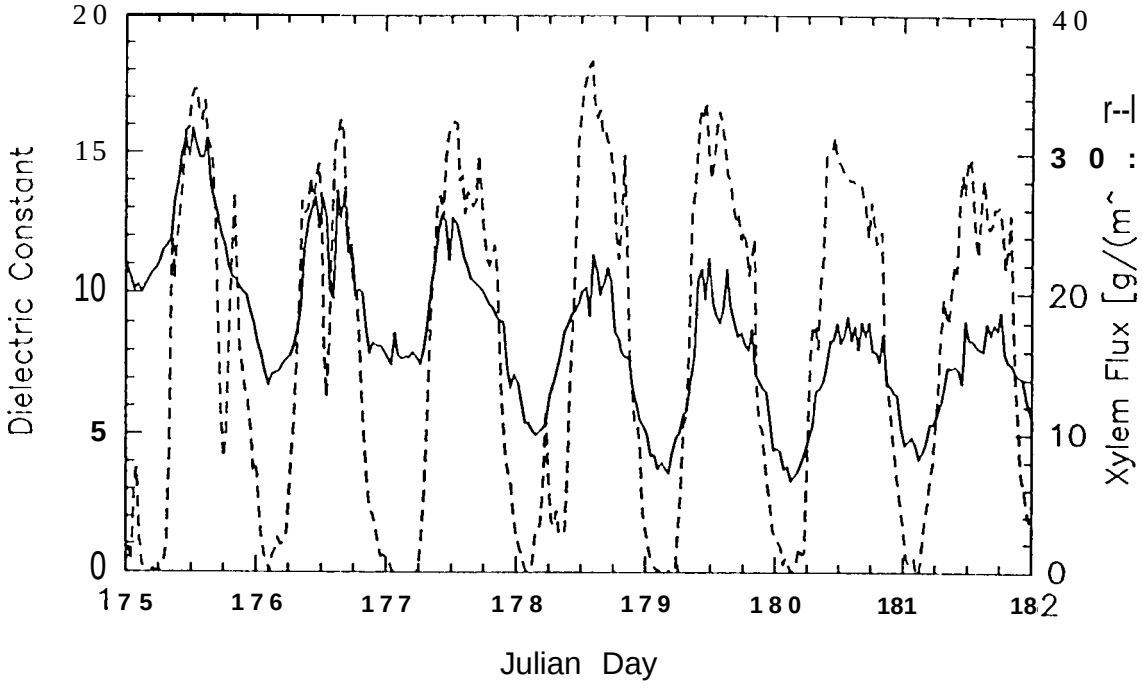
Dielectric Constant
Xylem Flux [g/(m^
Julian Day
0
5
10
15
20
0
10
20
30
40
175
176
177
178
179
180
181
182

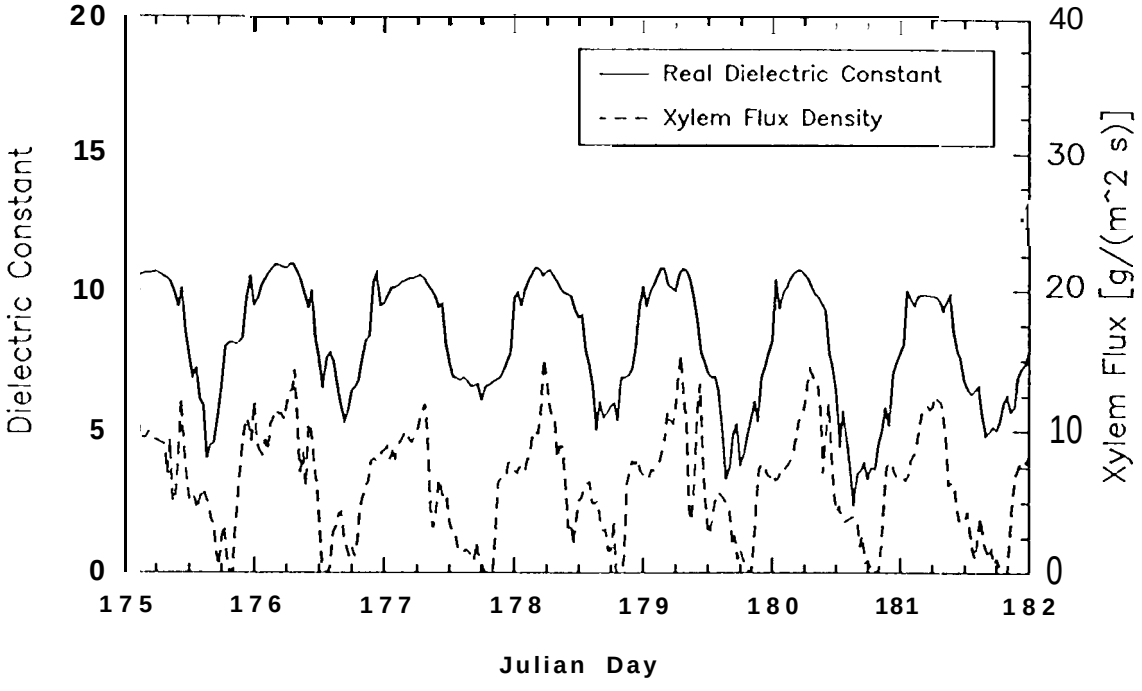
Real Dielectric Constant
Xylem Flux Density
Dielectric Constant
Xylem Flux [g/(m^2 s)]
Julian Day
0
5
10
15
20
0
10
20
30
40
175
176
177
178
179
180
181
182

Fig 11

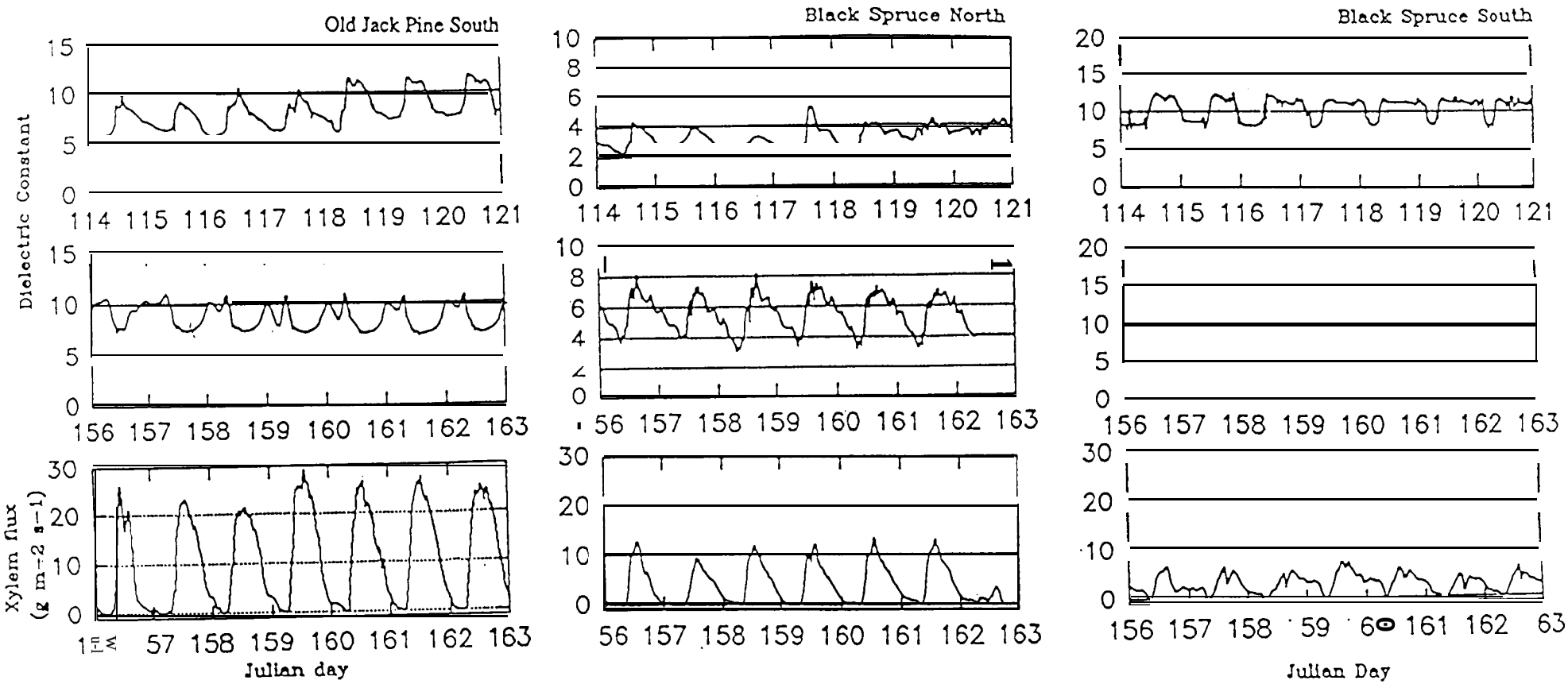
Old Jack Pine South
Black Spruce North
Black Spruce South
Dielectric Constant
Xylem flux
(g m-2 s-1)
Julian day
Julian Day

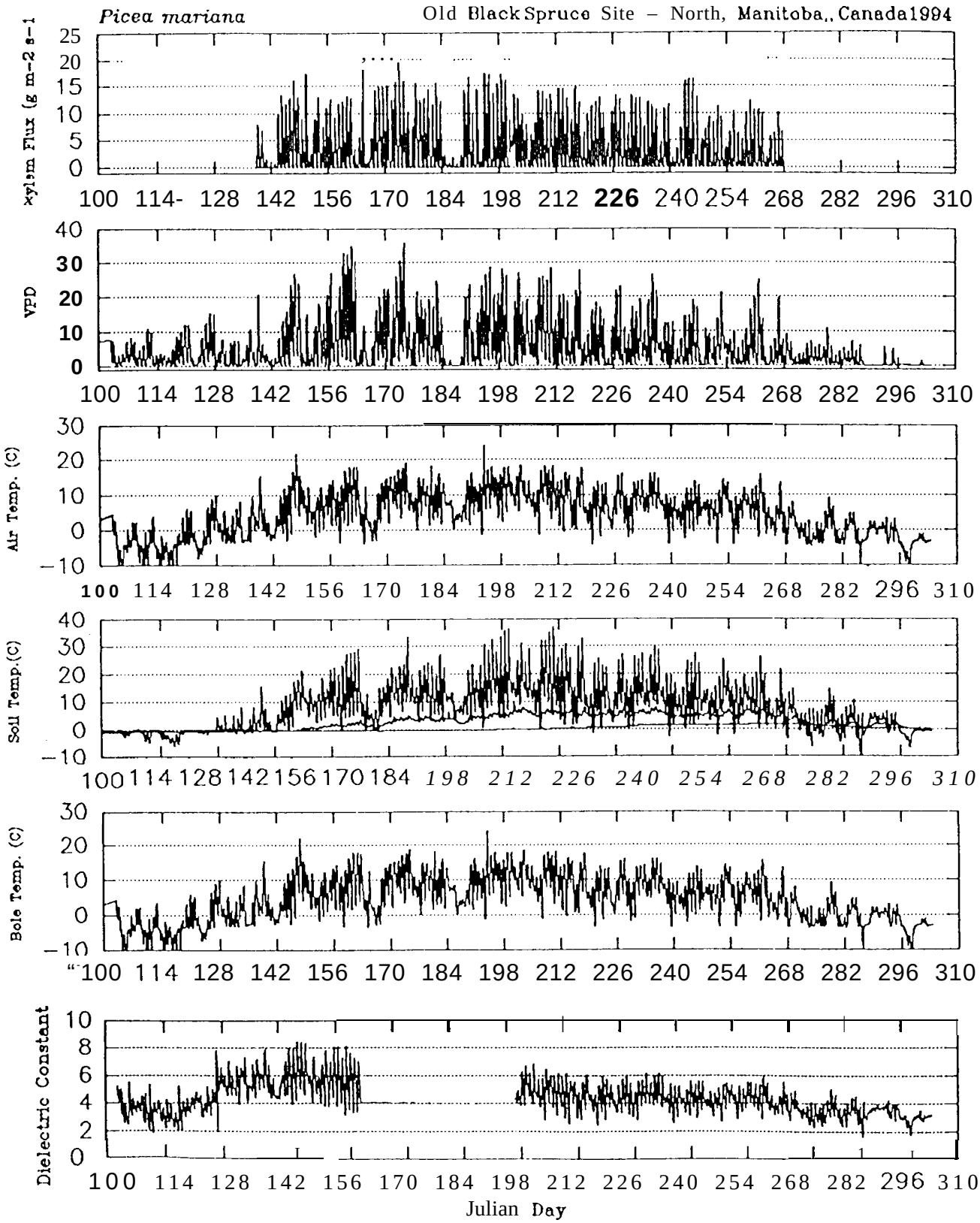
Picea mariana
Old Black Spruce Site – North, Manitoba, Canada 1994
Xylem Flux (g m-2 s-1
25
20
15
10
5
0
100 114 128 142 156 170 184 198 212 226 240 254 268 282 296 310
VPD
40
30
20
10
0
100 114 128 142 156 170 184 198 212 226 240 254 268 282 296 310
Air Temp. (C)
30
20
10
0
-10
100 114 128 142 156 170 184 198 212 226 240 254 268 282 296 310
Soil Temp.(C)
40
30
20
10
0
-10
100 114 128 142 156 170 184 198 212 226 240 254 268 282 296 310
Bole Temp. (C)
30
20
10
0
-10
100 114 128 142 156 170 184 198 212 226 240 254 268 282 296 310
Dielectric Constant
10
8
6
4
2
0
100 114 128 142 156 170 184 198 212 226 240 254 268 282 296 310
Julian Day

Fig 13

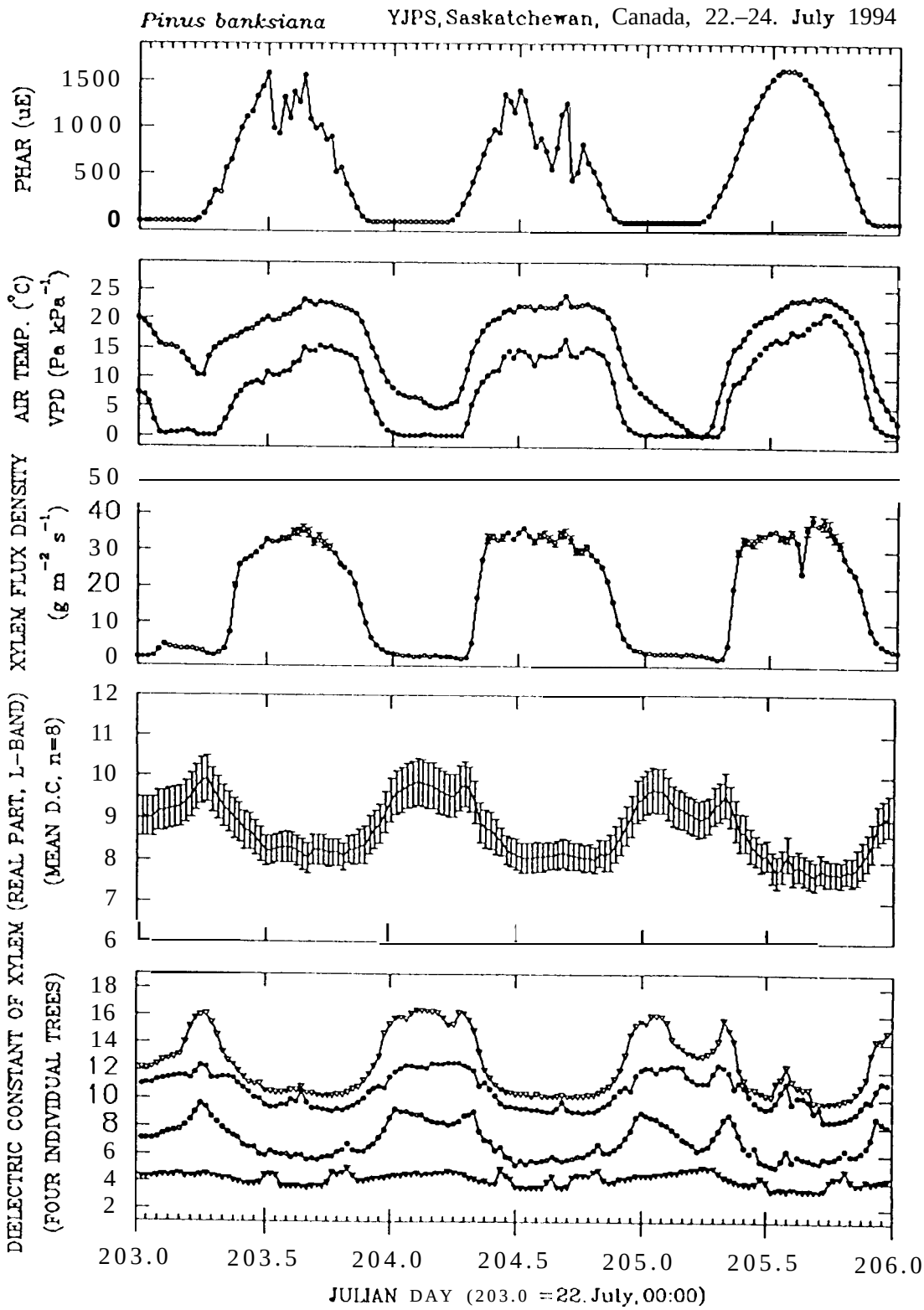
Pinus banksiana YJPS, Saskatchewan, Canada, 22.–24. July 1994
PHAR (uE)
1500
1000
500
0
AIR TEMP. (°C)
VPD (Pa kPa⁻¹)
25
20
15
10
5
0
XYLEM FLUX DENSITY
(g m⁻² s⁻¹)
50
40
30
20
10
0
DIELECTRIC CONSTANT OF XYLEM (REAL PART, L-BAND)
(MEAN D.C, n=8)
12
11
10
9
8
7
6
(FOUR INDIVIDUAL TREES)
18
16
14
12
10
8
6
4
2
203.0
203.5
204.0
204.5
205.0
205.5
206.0
JULIAN DAY (203.0 =22. July, 00:00)

Fig 14

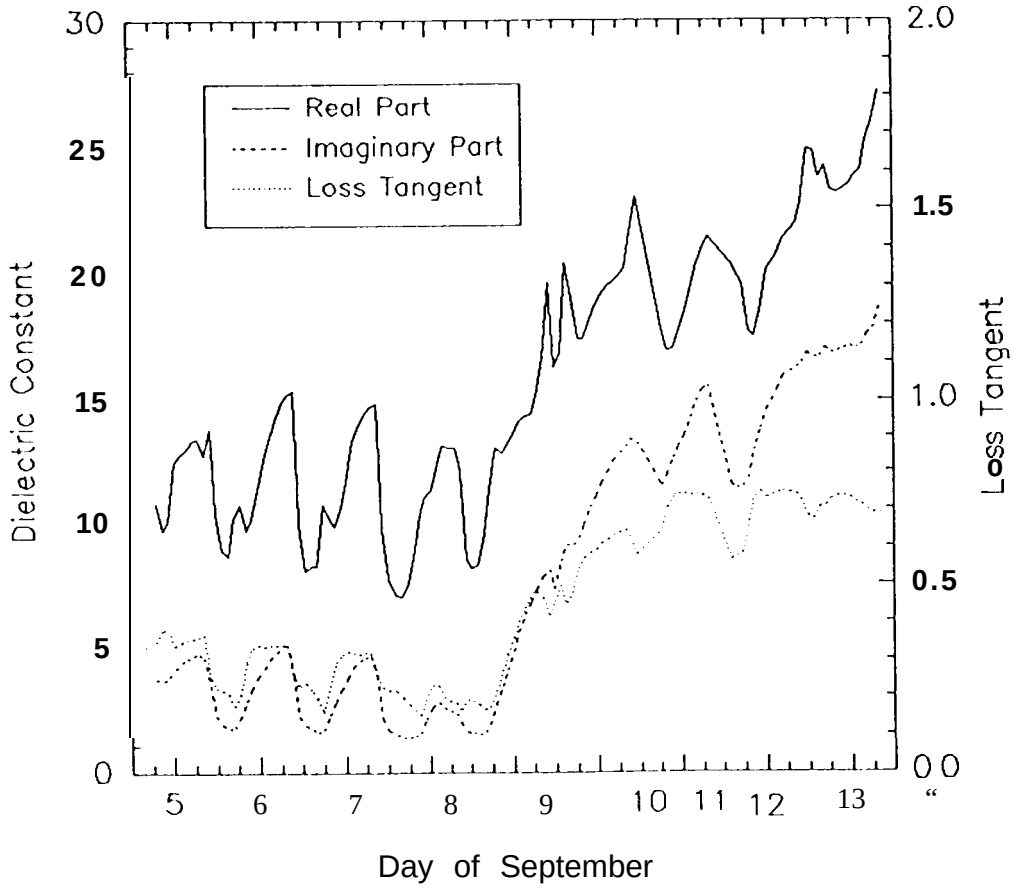
30
25
20
15
10
5
0
2.0
1.5
1.0
0.5
0.0
Real Part
Imaginary Part
Loss Tangent
Dielectric Constant
Loss Tangent
5
6
7
8
9
10
11
12
13
Day of September

Fig 15